REAL-TIME MONITORING AND CONTROL OF MECHANICAL FACE SEAL DYNAMIC BEHAVIOR

(Final Report Year 5)

Co-Investigator: Itzhak Green

The George W. Woodruff School of Mechanical Engineering
Georgia Institute of Technology

August 6, 2000
(Updated November 2003)

REAL-TIME MONITORING AND CONTROL OF MECHANICAL FACE SEAL DYNAMIC BEHAVIOR

Co-investigator: Itzhak Green (Georgia Tech)
Visiting Professor: Joshua Dayan (Technion – Israel Institute of Technology, March 1998 – February 1999)
Graduate Research Assistant: Min Zou (Ph.D., Graduated March 1999)
Graduate Research Assistant: Cody Casey (M.S., Graduated May 2000)

SUMMARY

Noncontacting mechanical face seals are extensively used in centrifugal pumps, compressors, powered vessels, and other high performance rotating machinery. Unpredictable mechanical face seal failure in critical applications may have severe implications. Added maintenance cost attributed to mechanical seal failure is much higher than the cost of just the seal itself. At the inception of this work the exact cause of seal failure as exhibited by higher harmonic oscillations (HHO) was not well understood. This research has determined that HHO are caused by the intermittent contact between the rotor and the stator (i.e., caused by an excessive relative face misalignment), leading to this harmful failure mode. Then, once such failure has been detected corrective measure have been implemented via active control to alter the system dynamics and eliminate the damaging behavior. Particularly, the techniques of monitoring, identification, and control developed in this research can be applied to water seals in Naval chillers, as well as other application that critically need to be monitored to increase their reliability and reduce maintenance cost. It is emphasized that since contact is determined ad hoc (i.e., phenomenologically) the technology developed here can be applied equally well to mechanical seals for compressible (gas/air) or incompressible (liquid) fluids. In addition, the existing mechanical face seal monitoring system has been utilized as a multi-fault monitoring system to also detect the presence of a transverse crack in the shaft upon which the seal is riding. A monitoring system that has the ability to detect multiple types of system failure has significant advantages including lower cost and simplification of the overall system.

Objective and Project Mission

This research consisted of two prongs:
(1) A Mechanical Seal Monitor: The objective here is to monitor and control the dynamic behavior of a noncontacting mechanical face seal having a flexibly mounted rotor in a seal test rig (see Figure 1). In particular, the research focuses on detecting and controlling the contact between the rotor and stator that may cause severe face wear and imminent seal failure. The condition monitoring system consists of three eddy current proximity probes and a universal controller board connected to a personal computer. The dynamic behavior of the noncontacting mechanical seal is monitored on-line. The monitoring system can display the orbit of the rotor angular misalignment in real-time where the shape of the orbit gives an indication of the seal dynamic behavior. Key dynamic parameters, such as seal clearance and relative angular misalignment between the rotor and the stator have been chosen to be monitored. Contact between the rotor and stator is detected by a combination of relative angular misalignment and seal clearance. A dominant indication of contact is the presence of higher harmonics oscillations, which are integer multiples of the rotating shaft speed. The monitoring system can detect seal contact during operation using orbit plots and signal processing, and suppress contact by incorporating an active control strategy. The control strategy is to eliminate contact between the rotor and the stator by adjusting the seal clearance. This is achieved by controlling a pneumatic air pressure in the rotor chamber, which governs the closing force. The fluid film stiffness and damping coefficients change with the clearance, thus a change in the clearance causes changes in the rotordynamic responses in both angular and axial modes.

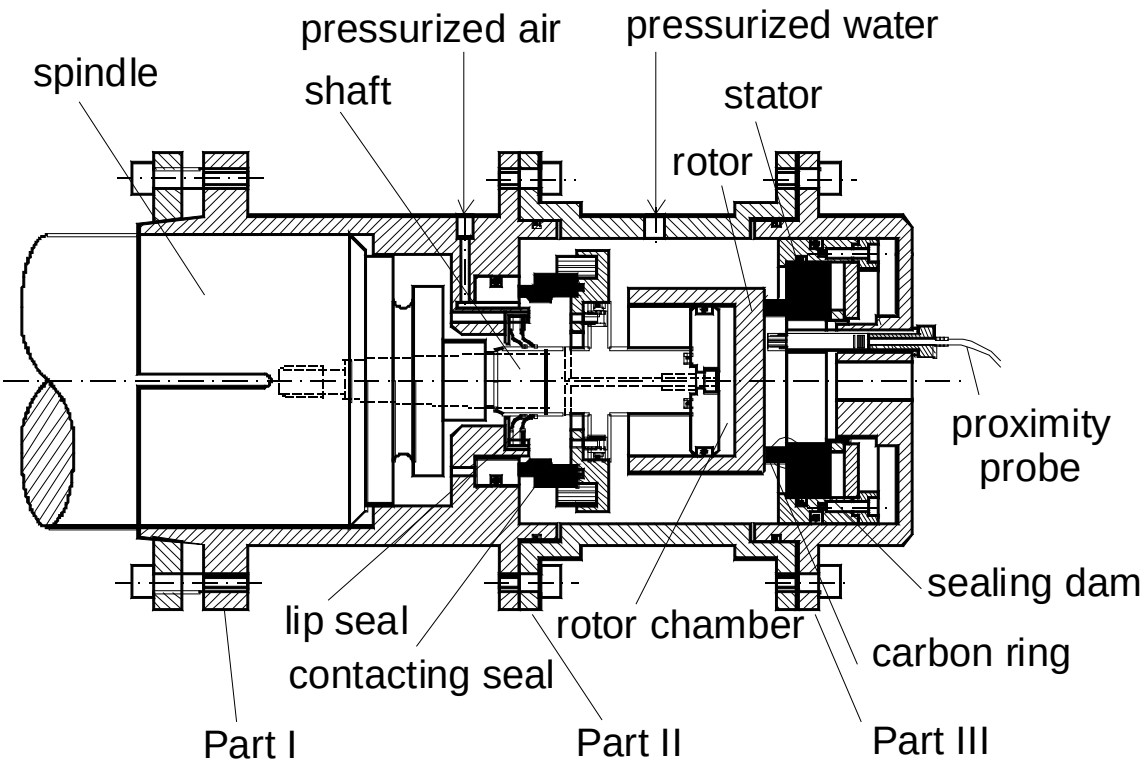

Figure 1. Schematic of the FMR noncontacting mechanical seal assembly

The seal clearance and the instantaneous rotor response are determined from signals of three eddy-current proximity probes. Contact is determined phenomenologically from pattern recognition of probe signals and their power spectrum densities as well as angular misalignment orbit plots, all calculated and displayed in real-time. The contact elimination strategy is experimentally investigated for various values of stator misalignment and initial rotor misalignment. Contrary to intuition, but compliant with the results of a parametric study, the experimental results show that for the seal under consideration contact can be eliminated through clearance reduction.

Approach

An experimental test rig has been built to study the dynamic response of a flexibly mounted rotor (FMR) mechanical face seal. This rig is being used to study higher harmonic oscillations because they have been detected under various operation conditions. A mechanical face seal that is designed to operate in a noncontacting mode may experience abnormal HHO, thus indicating the presence of rubbing contact between the rotor and stator. It is this contact that leads to face wear which obviously must be avoided. The seal system operates under the balance of the opening force and the closing force. The seal pressure drop provides the opening force across the sealing interface, while the sealed hydraulic pressure, the initial spring compression, and the air pressure in the rotor chamber provide the closing force. Initially the air pressure was set manually by a pressure regulator and was not automatically controlled. Subsequently an electro-pneumatic transducer automatically adjusted the pneumatic pressure in the rotor chamber, and thus adjusted the closing force acting on the flexibly mounted rotor. The monitoring system based on the eddy-current proximity probes and a flow meter has been used to monitor the rotordynamic behavior and detect the presence of HHO. The flow meter outputs a voltage that is proportional to the flow rate. Ultimately a control algorithm on the closing force was incorporated. Once contact was detected the control system altered the system dynamics to reduce the relative misalignment between rotor and stator for maximum reduction of HHO.

(2) Crack Detection in Seal Driving Shaft[1]: As rotating machinery is designed to operate at higher mechanical efficiency, operating speeds, power, and loads are increased as weight and dimensional tolerances are decreased. The result is a significantly increased level of operating stress in modern rotating machinery. As a consequence of this increased stress level, many practical rotor dynamic systems contain shaft/rotor elements that are highly susceptible to transverse cross-sectional cracks due to fatigue. Vibration monitoring of rotating machinery has become common practice in many industries involving turbines, generators, pumps, and other types of rotating systems. Various types of transducers and monitoring systems are utilized by operators to measure, monitor, and diagnose system faults such as shaft out-of-balance or misalignment, damaged roller bearings, loose bearings, oil film whirl, damaged gear or belt drives, etc.

Early detection of mechanical malfunction is essential. Not only can a catastrophic failure be avoided, given adequate warning of plant failure, arrangements for equipment repair or replacement can be made and efficiently carried out to minimize the amount of time the machine is off-line. Vibration monitoring also has the significant advantage of usually requiring no disassembling of the system components. On-line methods can be implemented without even taking the system out of use. A monitoring system that has the ability to detect multiple types of system failure has significant advantages including lower cost and simplification of the overall system. This work explores the feasibility of utilizing an existing seal monitoring system to detect an additional type of system fault, in particular the presence of a crack in the seal-driving shaft.

Approach

The existing monitoring system has the ability to detect seal face contact in a flexibly mounted rotor (FMR) mechanical face seal, by directly monitoring the dynamic response of the rotor, and eliminate or reduce the severity of the contact with real-time active control. The primary objective of here is to explore the feasibility of utilizing the existing mechanical face seal monitoring system to detect a transverse crack in the shaft of the test rig. This research has focused on developing a fundamental understanding of and detecting a shaft crack in the system using the existing seal monitoring system. Ultimately, crack detection results could be used in conjunction with the seal face contact detection results to develop a multi-fault detection system.

To accurately predict the response of a system to the presence of a transverse crack, an appropriate crack model is essential. Once the crack is included in the system model, unique characteristics of the system response can be identified and attributed directly to the presence of the crack. These predicted indicators then serve as target observations for the monitoring system.

a. Theoretical Analysis

This research utilizes a global asymmetry crack model in a continuous representation of the system as well as a gaping crack model in a discrete representation of the system. The theoretical analyses focus on the prediction of the behavior of an induced 2X component in the system response. The global asymmetry crack model analysis approximates the stiffness of the cracked shaft with the stiffness of a shaft whose cross-section, for the entire length of the shaft, is identical to the uncracked cross-section at the location of the crack. The local asymmetry crack model utilizes a transfer matrix method to discretize the system so that the additional flexibility introduced by the presence of the crack is localized along the axis of the shaft. Free and forced response analyses were used to identify characteristics of the system response that can be directly attributed to the presence of a crack in the shaft of the system.

The free response analyses yield plots of the natural (whirl) frequencies of the system as a function of shaft speed for various crack depths. Plots obtained for both crack models show the natural frequencies of the system as a function of the shaft speed for crack depths up to 40% of its diameter. Shaft speeds at which a resonance type behavior in the 2X harmonic component of the system response can be predicted from these free response analyses.

---

[1] Prong 2 was not part of the original proposal. It was added to the work upon accomplishing the objectives stated in prong 1 towards end of year 4.

The decrease in the 2X resonance shaft speeds for an increasing crack depth indicates a decrease in the natural frequencies of the system, and can serve as a first indicator of a crack in the shaft of a system.

Then the forced response analyses provide a prediction of the behavior of the magnitude of the 2X component of the response of the system. Analysis reveals a decrease in 2X resonance speeds for increasing crack depth, as well as an increase in the magnitude of the 2X component at resonance. These behaviors of the system forced responses are predicted to serve as second indicators of a shaft crack in the system.

b. Experimental Analysis

In the seal experiments the shaft was made particularly stiff to monitor the behavior of the flexibly mounted seal alone. Here experiments were performed utilizing a modified test rig and a manufactured crack to verify the predicted behavior of the 2X harmonic component of the system response. The shaft was made slender (i.e., flexible) but the rotor was rigidly attached to the shaft. Since higher harmonic components of the system response are always present in a realistic system, the behavior of the 2X component of the system response is experimentally obtained for uncracked and various cracked cases so that relative changes in system response components can be observed. A single shaft was used in the experiments. The crack was incrementally deepened incrementally (using EDM at width of 0.3 mm) for each data set up to 40% of the shaft diameter.

The experimental results qualitatively confirm the behavior of a meaningful 2X harmonic component of the response of the cracked system that was predicted in the theoretical analyses. The decrease in 2X resonance speeds for increasing crack depth, as well as an increase in the magnitude of the 2X component at resonance could clearly be observed.

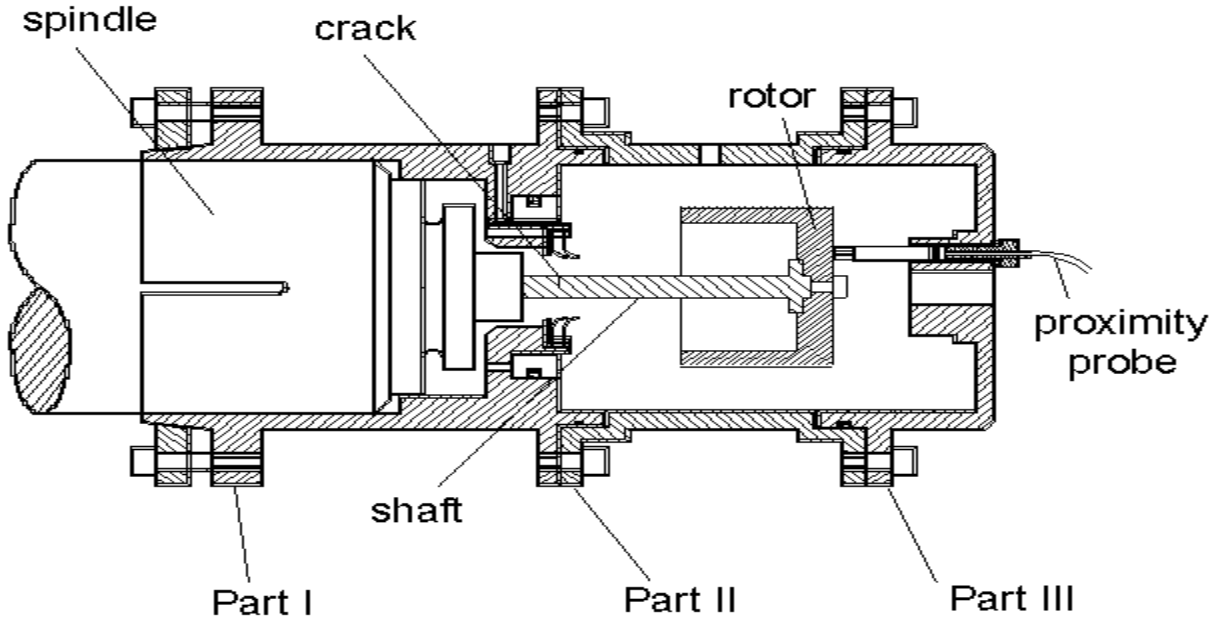

Figure 2. Schematic of a cracked shaft in the same mechanical seal assembly

Results/Accomplishments

1. Dynamic Simulation and Monitoring of a Flexibly Mounted Rotor Face Seal

The rotordynamics has been investigated through both, simulation and real-time monitoring. Dynamic simulation has been performed to investigate the seal rotor angular response to the stator misalignment, the stator angle, the initial rotor misalignment, and clearance. Rotor angular response orbit has been introduced, capable of characterizing the rotor dynamic response. A real-time monitoring system has been constructed in the test rig to monitor the instantaneous dynamic behavior of the seal rotor including its angular response, precession angle, and angular response orbit. Experimental results agree well with those of the dynamic simulation.

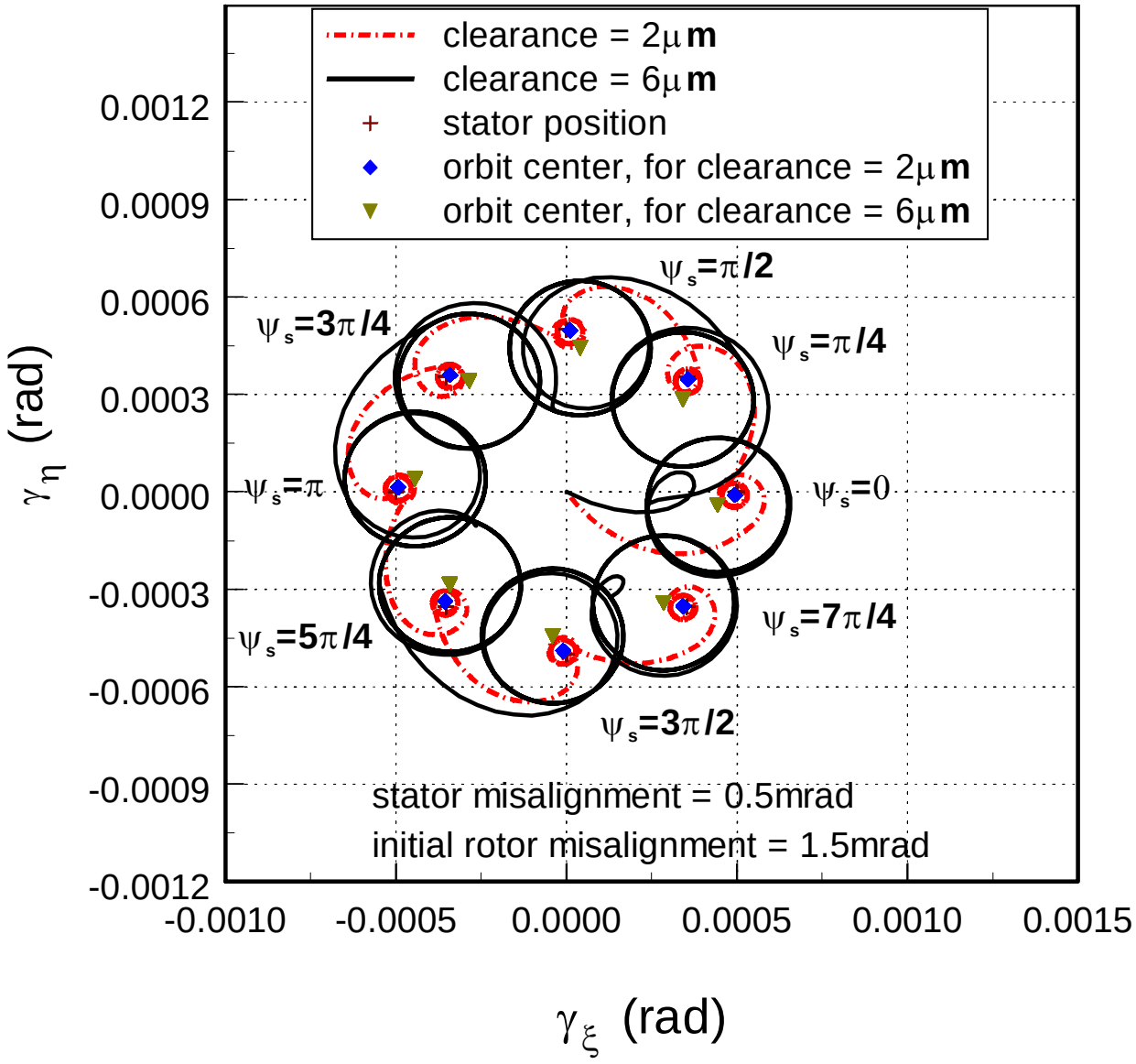

Fig. 3: Simulated rotor angular response orbits at various stator angles, for two seal clearances

The ability for the rotor to track the stator misalignment, γ_s, and stator angle, ψ_s is investigated. The stator misalignment (in this example) is set to 0.5 mrad. The initial rotor misalignment is arbitrarily set to 1.5 mrad, a value that is different from stator misalignment. These values are typical for real seal applications. In reality the stator angle is fixed but it can assume any value between 0 and 2π. Therefore, in the simulation the stator angle is checked for different values between 0 and 2π, at $\pi/4$ steps, every 0.2 s intervals, and for two different clearances, 2 μm and 6 μm. The simulation results are plotted in Figs. 3, which shows the rotor angular response orbit as it changes with various stator angles and two clearances. The simulation starts at the origin, $\gamma_\xi = \gamma_\eta = 0$. The steady-state rotor angular response orbit is a circle centered at the point whose polar coordinates are the mean value of the rotor misalignment (the magnitude) and the mean value of rotor precession (the angle). This point, for the parameters investigated here, is close to another point whose polar coordinates are the stator misalignment and the stator angle, ψ_s. The distance between the two points depends on various seal parameters, such as, clearance, the smaller the clearance the smaller the distance. The mean value of the rotor misalignment is γ_{rs}. The variation of the rotor misalignment about its mean value is $\gamma_{rI.}$ The simulation is shown as a continuous plot; however, each orbit represents a specific condition. This will now be shown to correlate well with the monitoring results from specific experiments.

Because clearance is a very important parameter in seal operation, its effect on rotor response is further investigated. Figs. 4a – 4c show the simulation results for stator misalignment of γ_s=0.5 mrad, while Figs. 5a –5c show the simulation results for γ_s=1.5 mrad. The chosen values of ψ_s for the simulation match those of the experimental results, which follow later. The simulation results are plotted for two different initial rotor misalignments, 0.5 mrad and 1.5 mrad, at six clearances ranging from 1 μm to 6 μm. The clearance is changed at time intervals of 0.2 s, in a scheme that can be implemented physically in the test rig for the purpose of clearance control (accomplished and described subsequently).

It can be seen from Figures 4a and 5a that the ability of the rotor precession angle, ψ_r, to follow the stator angle, ψ_s, varies with clearance. The precession angle better adapts to the stator angle and results in smaller oscillation amplitude as the clearance decreases. The precession angle amplitude also depends on the initial rotor misalignment, the smaller the initial misalignment the smaller the amplitude. By comparison it can be seen that when the stator misalignment is smaller (Fig. 4a), the rotor precession angle tracks the stator angle closer but with a larger amplitude.

Similar conclusions can be drawn from Fig. 4b and Fig. 5b for the rotor misalignment, γ_r. This misalignment better adjusts itself to the stator corresponding misalignment of γ_s = 0.5 mrad or 1.5 mrad, when γ_s is smaller. The oscillation amplitudes decrease with the clearance. The amplitudes also depend on the initial rotor misalignment, γ_{ri}, where the smaller the initial misalignment the smaller the amplitude. Comparison of Fig. 4b and Fig. 5b also shows that when the stator misalignment is smaller (Fig. 4b), the rotor misalignment tracks the stator misalignment more closely. The amplitude of the rotor misalignment is essentially the same for both values of stator misalignment.

Fig. 4c and Fig. 5c show the rotor angular response orbits for the two stator misalignments of 0.5 mrad and 1.5 mrad, respectively, at two different initial rotor misalignments, 0.5 mrad and 1.5 mrad, and six clearances. For both initial rotor misalignments cases shown, the radius of the orbit decreases when the clearance decreases. While the loci of orbit centers is not shown in the figures, the results are such that when the clearance decreases the center of the orbit also moves towards the point whose polar coordinates are the stator misalignment and the stator angle. An interesting phenomenon is that when the initial rotor misalignment is equal to (or close to) the stator misalignment, i.e., γ_{ri} = 0.5 mrad in Fig. 4c, and γ_{ri} = 1.5 mrad in Fig. 5c, the rotor response orbits for different clearances pass through a common point. Therefore, for practical monitoring purposes dynamic responses that pass through the same point indicate that the stator and initial rotor misalignment are close to each other.

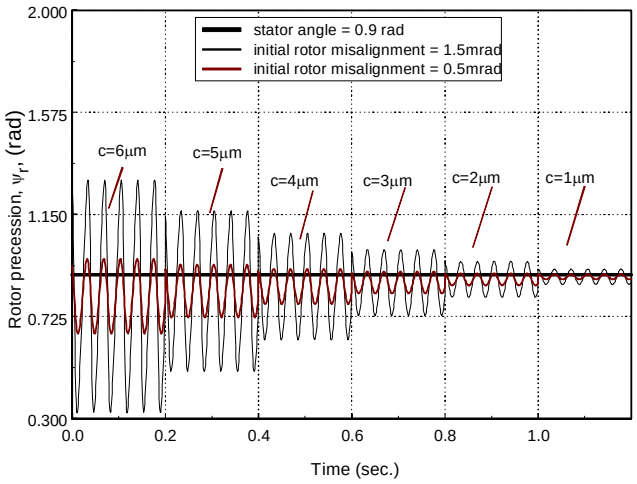

Fig. 4a Simulated rotor precession vs. time for changes in seal clearance (stator misalignment = 0.5 mrad, stator angle = 0.9 rad, initial rotor misalignment = 0.5 mrad and 1.5 mrad)

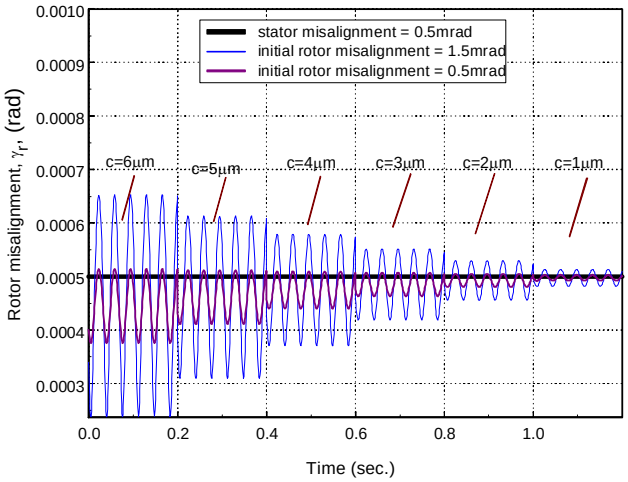

Fig. 4b Simulated rotor misalignment vs. time for changes in seal clearance (stator misalignment = 0.5 mrad, stator angle = 0.9 rad, initial rotor misalignment = 0.5 mrad and 1.5 mrad)

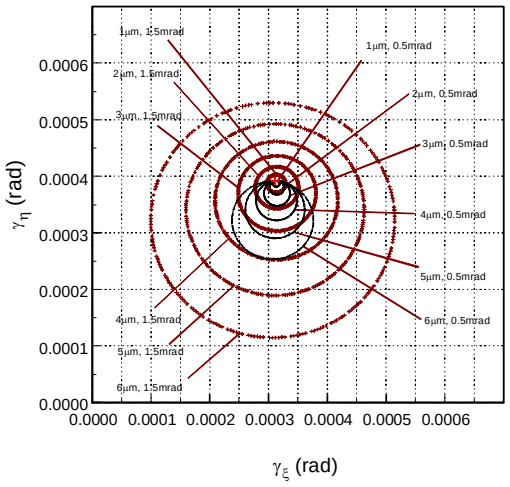

Fig. 4c Simulated rotor angular orbit plot for changes in seal clearances (stator misalignment = 0.5 mrad, stator angle = 0.9 rad, initial rotor misalignment = 0.5 mrad and 1.5 mrad)

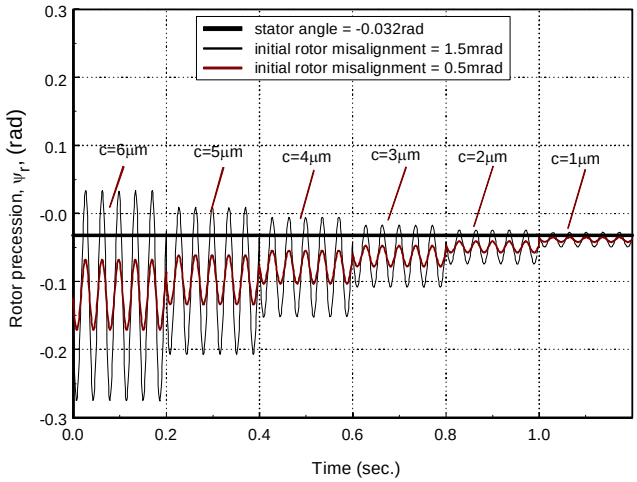

Fig. 5a Simulated rotor precession vs. time for changes in seal clearance (stator misalignment = 1.5 mrad, stator angle = -0.032 rad, initial rotor misalignment = 0.5 mrad and 1.5 mrad)

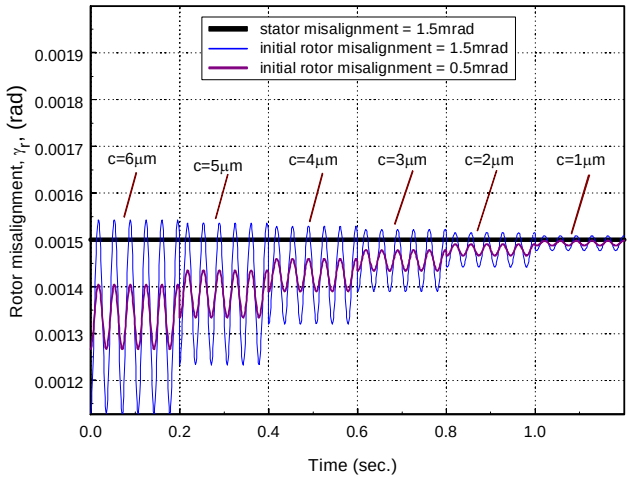

Fig. 5b Simulated rotor misalignment vs. time for changes in seal clearance (stator misalignment = 1.5 mrad, stator angle = -0.032 rad, initial rotor misalignment = 0.5 mrad and 1.5 mrad)

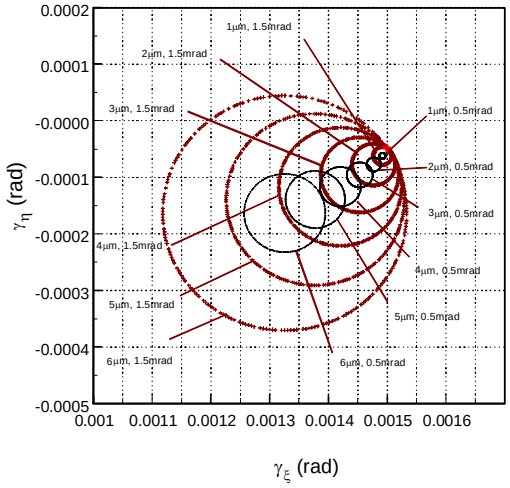

Fig. 5c Simulated rotor angular orbit plot for changes in seal clearances (stator misalignment = 1.5 mrad, stator angle = -0.032 rad, initial rotor misalignment = 0.5 mrad and 1.5 mrad)

The monitoring system

Three eddy current proximity probes mounted on the end of the housing are used to detect the instantaneous dynamic response of the rotor. These proximity probes have a bandwidth of about 10 kHz. They can measure the static and dynamic distances between their tips and the rotor end surface. A low pass filter with a cut-off frequency of 1 kHz is used to eliminate high frequency cross-talk noises among the probes and also to serve as an anti-aliasing filter. The maximum output of each proximity probe is -24 V. A voltage divider is used to drop the

maximum amplified voltages of the proximity probes outputs from -24 V to -10 V. The reduced voltages are then sent into a universal board that is mounted in a personal computer. The board has a floating-point Digital Signal Processor (DSP). The DSP has been supplemented by a set of on-board peripherals, such as analog to digital (A/D) and digital to analog (D/A) converters. The proximity probe signals are obtained through the A/D converter of the board. A flow meter is also used to measure the leakage of the seal. The proximity probe signals and leakage measurement are then processed by the on-board DSP and the results are sent to the computer in real-time for on-line display or for data recording. Key dynamic parameters, such as the rotor misalignment, the rotor precession angle, the rotor angular response orbit, and the clearance are monitored.

Real-time Monitoring

The sealed water pressure is set to 345 kPa, and the shaft speed is 28 Hz. The graphite stator in the stator assembly is deformed to provide a coning angle of 1 mrad. The monitored parameters are the same as those in the dynamic simulations, i.e., the rotor misalignment, the rotor precession angle, and the rotor angular response orbit. Two sets of experimental results are described in Figures 6 and 7. These are then compared qualitatively with the simulations of Figures 4 and 5, respectively.

The first set of experimental results for four different clearances are presented in Fig. 6. The procedure for taking experimental data is: setting the air pressure in the rotor chamber to 27.6 kPa, running the shaft at 28 Hz and recording the monitored data; repeating this procedure by incrementing the air pressure (by approximately 14 kPa) to 41.4kPa, then 55.2 kPa, and lastly 69.0kPa. From the leakage measurement (see Fig. 6e) the clearances are calculated to be 6μm, 2.8μm, 1.5μm, and 0.5μm, respectively. Also, from the three proximity probes signals (Fig. 6d) the stator misalignment and angle are calculated to be 0.5 mrad, and 0.9 rad, respectively. The second set of experimental results is obtained by the same procedure (Fig. 7). This time, however, tests are conducted for six decreasing clearances from 6μm to 1μm, in increments of 1μm. Again, Fig. 7e depicts the clearances as calculated from the leakage measurement. Fig. 7d shows the three proximity probe signals from which the stator misalignment of 1.5 mrad and the stator angle of –0.032 rad (cyclically equivalent to 6.251 rad) are calculated.

As stated, the rotor response is a function of the initial rotor misalignment as well as the stator misalignment. The simulations in Section 2 pertain to the four combinations of stator and initial rotor misalignments of 0.5 and 1.5 mrad. The purpose of the physical testing is to verify the seal dynamic behavior experimentally under similar conditions. However, it should be noted that the initial rotor misalignment is set only once, at the beginning of each set. In the execution of the successive runs for the different clearances the initial rotor misalignment assumes some value affected by both the previous run and the amount of relaxation present in the two O-rings, which form the flexible rotor support. Therefore, the rotor gradually adjusts itself to the stator misalignment and the initial rotor misalignment is not fixed as theoretically assumed, but varies each time the system runs and stops (i.e., between clearance changes). Consequently, only the first run in each set of experiments nearly corresponds to the assumed initial rotor misalignment used in the simulation (γ_{rI}=1.5 mrad for C=6 μm in Fig. 6 and γ_{rI}=0.5 mrad for C=6 μm in Fig. 7). All the other experimental results fit only qualitatively to the simulated ones, exhibiting better dynamic responses because of an effectively decreasing initial rotor misalignment at the beginning of each test. The outcome of which are smaller final rotor misalignments, displaying tighter rotor response orbits.

Figures 6a and 6b depict, respectively, the changes in the rotor precession angle and the rotor misalignment with the clearance. Both the rotor precession angle and the rotor misalignment vary periodically and their amplitude decreases as the seal clearance decreases. A similar behavior is displayed by Fig. 4a and 4b for initial rotor misalignment of 1.5 mrad. The large peak to peak amplitude at the beginning of the operation is due to the large initial rotor misalignment with respect to the stator misalignment (0.5 mrad). As explained, the rotor gradually adjusts itself to the stator misalignment as the clearance decreases and both the rotor precession angle and misalignment amplitudes are also reduced. The mean value of the rotor precession angle approaches the stator angle and the rotor misalignment approaches that of the stator (its behavior becomes similar to Fig. 4b for initial rotor misalignment of 0.5 mrad). The same phenomenon is observed by comparing Fig. 6c with Fig. 4c. They show the rotor angular response orbits for different clearances in both experiments and in simulation. As expected the

orbits approach circular shapes. The smaller the clearance the smaller the orbit size, and the orbit centers approach the point whose polar coordinates are the stator misalignment and the stator angle. At the beginning of the experiment, for the clearance of 6μm, the initial rotor misalignment (presumably 1.5 mrad) is not close to the stator misalignment (0.5 mrad). With the decrease of the clearance at the beginning of each test, the initial rotor misalignment reduces as well. Therefore, the experimental orbits (Fig. 6c) are intersecting having a behavior between the two extremes of the simulated orbits of Fig. 4c. It should be pointed out that the center of the orbit has polar coordinates defined by the average of the maximum and minimum of the rotor misalignment, and the average of the maximum and minimum of the rotor precession angle. These averages eventually approach the point defined by the stator misalignment and stator angle.

Results obtained from the second set of experiments (Fig. 7) are similar in nature, although the stator and initial rotor misalignments are reversed (γ_s=1.5 mrad and γ_{rI}=0.5 mrad for C=6 μm). Again, the rotor precession angle is cyclic and its amplitude decreases as the seal clearance decreases (Fig. 7a). This behavior is qualitatively similar to Fig. 5a for initial rotor misalignment of 0.5 mrad. Likewise, the rotor misalignment is also periodic and its amplitude decreases as the seal clearance decreases (Fig. 7b). Since its behavior is similar to Fig. 5b (for initial rotor misalignment of 0.5 mrad) it may suggest that the initial rotor misalignment is indeed about 0.5 mrad and effectively remains constant between tests (even for smaller clearances). Comparing Fig. 7c and Fig. 5c shows the resemblance between the experimental orbits and those of the simulation for initial rotor misalignment of 0.5 mrad. Similarly, the clearances calculated from the proximity probe signals (Fig. 7d) match very well (within a few percents) the clearances calculated from the leakage (flow rate) measurements (Fig 7e).

FFT analyses performed on both experimental sets (Figs. 6d and 7d) reveal very minor second higher harmonic components in the eddy current proximity probe signals for all the tested clearances, indicating that there is no contact between the seal faces. Also the similarity between the experimentally obtained orbits and the numerically simulated orbits (the latter are based upon a noncontacting analytical model) further support the conclusion that the seal operates in a noncontacting mode.

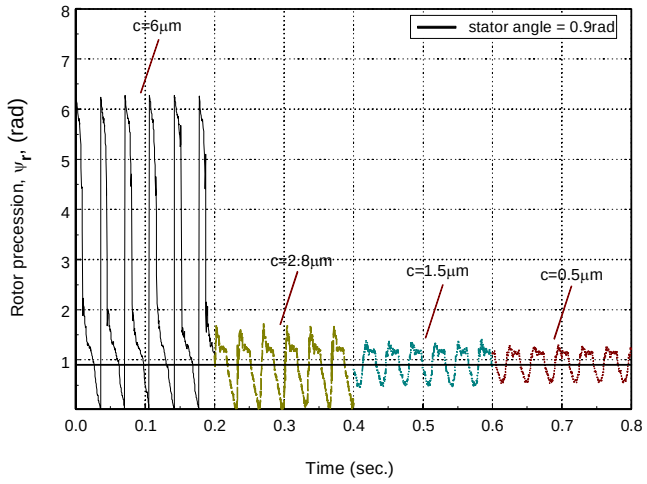

Fig. 6a Experimental rotor precession vs. time for changes in seal clearance (stator misalignment = 0.5 mrad, stator angle = 0.9 rad)

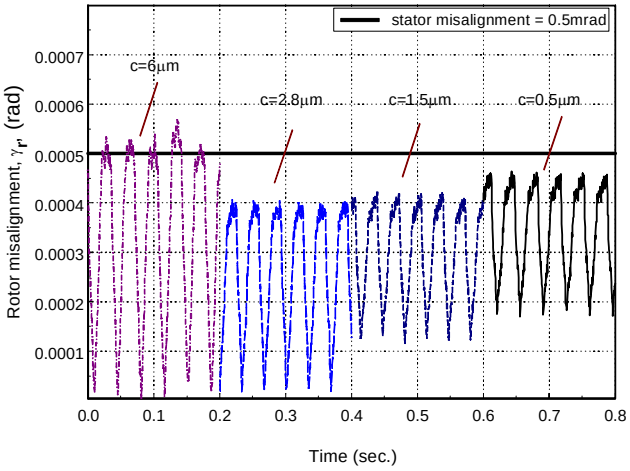

Fig. 6bExperimental rotor misalignment vs. time for changes in seal clearance (stator misalignment = 0.5 mrad, stator angle = 0.9 rad)

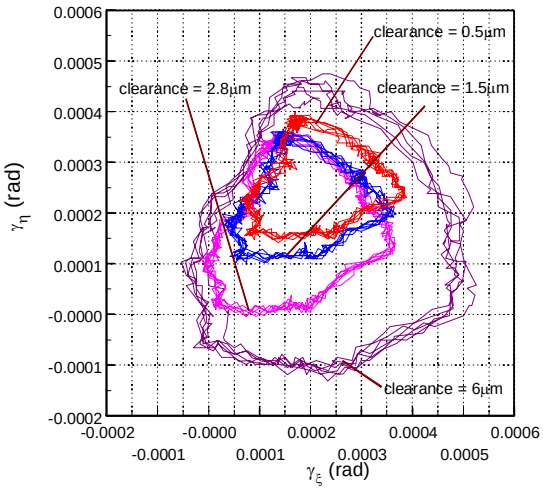

Fig. 6c Rotor angular misalignment orbit changes with seal clearance (stator misalignment = 0.5 mrad, stator angle = 0.9 rad)

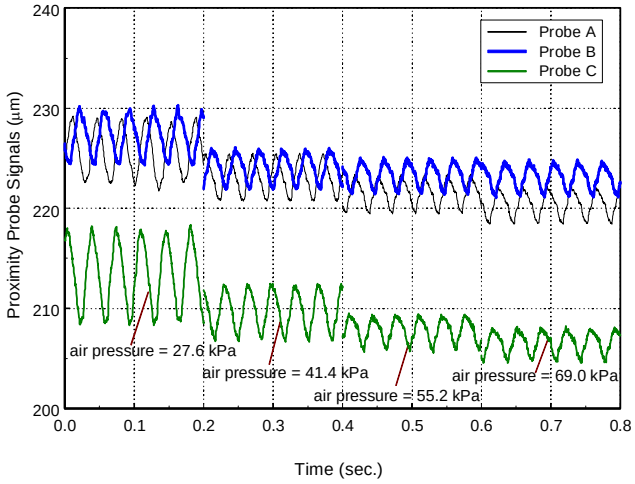

Fig. 6d Proximity Probe signals vs. time (stator misalignment = 0.5 mrad, stator angle = 0.9 rad)

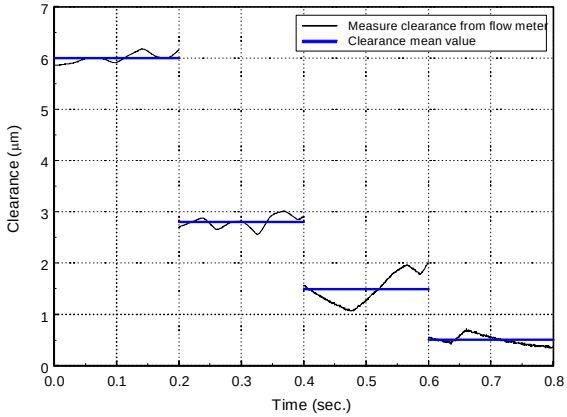

Fig. 6e Clearance measured by flow meter vs. time (stator misalignment = 0.5 mrad, stator angle = 0.9 rad)

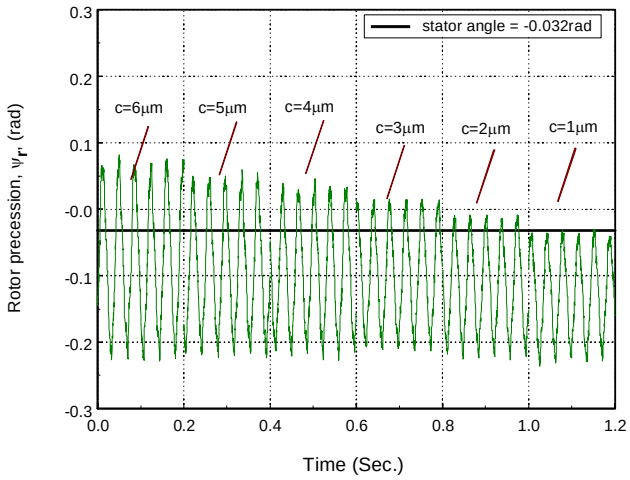

Fig. 7a Experimental rotor precession vs. time for changes in seal clearance (stator misalignment = 1.5 mrad, stator angle = -0.032 rad)

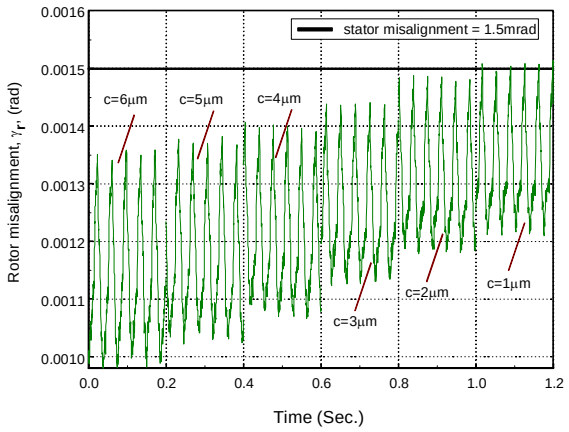

Fig. 7b Experimental rotor misalignment vs. time for changes in seal clearance (stator misalignment = 1.5 mrad, stator angle = -0.032 rad)

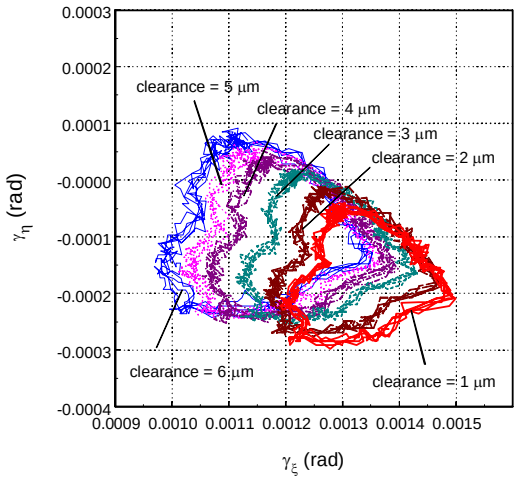

Fig. 7c Rotor angular misalignment orbit changes with seal clearance (stator misalignment = 1.5 mrad, stator angle = -0.032 rad)

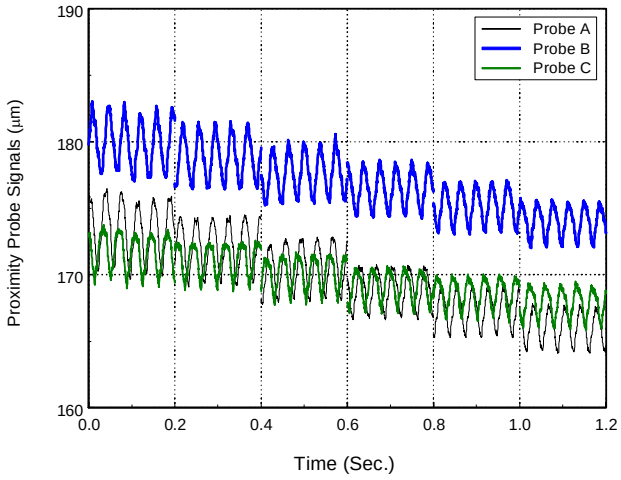

Fig. 7d Proximity Probe signals vs. time (stator misalignment = 1.5 mrad, stator angle = -0.032 rad)

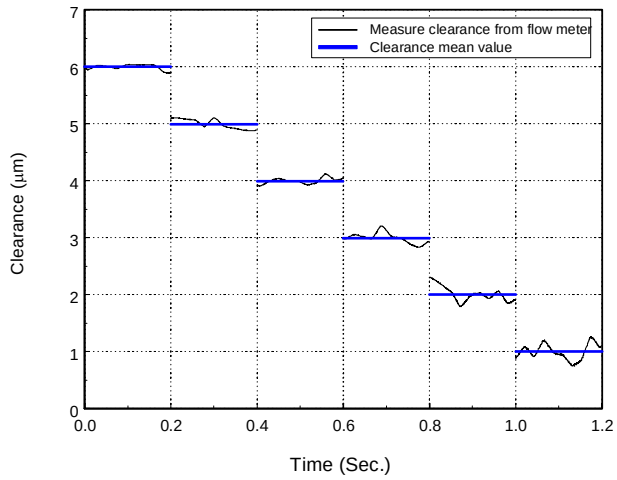

Fig. 7eClearance measured by flow meter vs. time (stator misalignment = 1.5 mrad, stator angle = -0.032 rad)

Dynamic simulation is performed using the parameters of a noncontacting FMR mechanical face seal test rig. A monitoring system is constructed to monitor the dynamic behavior of the seal in real-time. The similarities between the simulation and monitoring results clearly indicate that the seal dynamic model established captured the major dynamic behavior of the seal. Any subtle differences between the simulation and the monitoring results could have been caused by unavoidable experimental uncertainties, or by the small perturbation assumption made in the development of the analytical model. The fact that the experimental results cover a large range of clearances, which is beyond the small perturbation range, gives more confidence in applying this model to a larger clearance range. The rotor angular misalignment orbit is found to contain information related to the rotor angular response, rotor precession angle, and the stator misalignment and stator angle.

When a seal operates in noncontacting mode the seal rotor dynamic behavior could be better understood by comparing the dynamic monitoring and the simulation results. If contact occurs the monitored rotor response would be visibly different from the simulated response because the simulation is based upon a noncontacting analytical model. It is expected that the sensors signal will be corrupted by noise and vibration generated by the face contact and the misalignment orbit will deviate substantially from the smooth circular one predicted by the simulation for the noncontacting case. Therefore, the monitoring system can potentially function also as a detection system of seal face contact.

A more advanced and proactive step in face seal dynamics is to control the seal rotordynamic behavior and prolong its life. A control system that can take meaningful action based on the real-time dynamic monitoring and contact detection results is now being described.

2. Clearance Control

Seal clearance control is an advancement in noncontacting mechanical face seal operation because seal clearance variation caused by process disturbances may cause either severe face contact or excessive leakage, each of which is regarded as seal failure. The objective of controlling the seal clearance at a desired value overcoming operation disturbance, including variations in shaft speed and sealed fluid pressure, has been accomplished. The clearance control concept is to adjust the closing force that acts upon the flexibly mounted rotor. The seal axial dynamic

model has experimentally been determined for the design of a proportional-integral (PI) controller with anti-windup. The controller has been then applied to the test seal. Results have shown that the controlled seal maintains or follows set-point clearance changes with and without disturbances in sealed water pressure and shaft speed (Figure 8). The controlled seal has been shown to respond quickly (having a small time constant) with a small control effort.

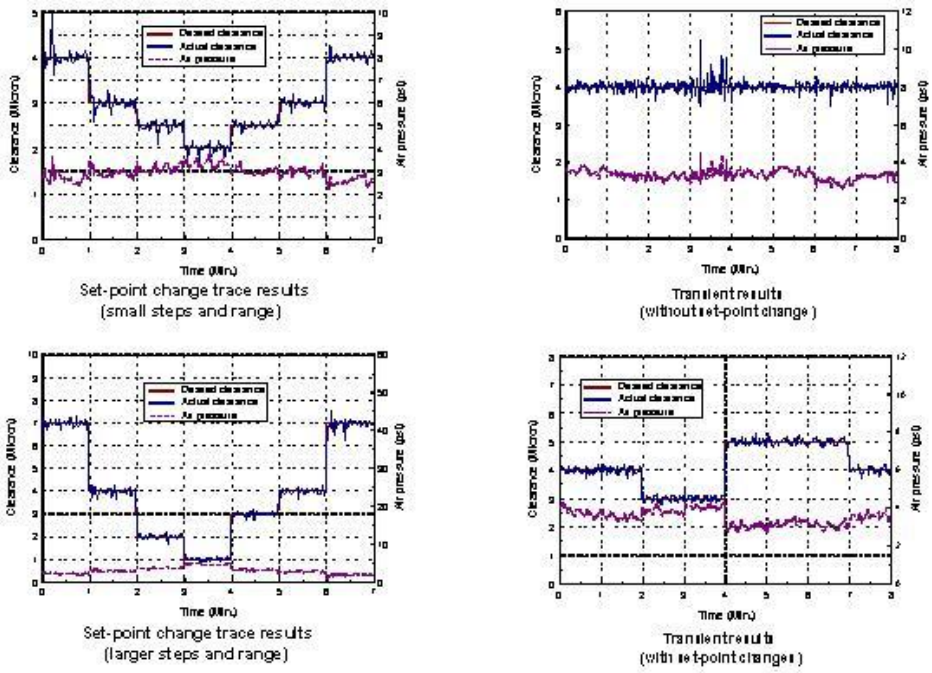

Figure 8. Seal clearance control results

3. Feasibility of Contact Elimination through Clearance Adjustment

The feasibility of eliminating contact in a noncontacting flexibly mounted rotor (FMR) mechanical face seal has been studied. The approach for contact elimination is based on a parametric study using FMR seal dynamics. Through clearance adjustment it is possible to reduce the maximum normalized relative misalignment between seal faces and, therefore, eliminate seal face contact. Contact has been determined phenomenologically from pattern recognition of probe signals and their power spectrum densities as well as angular misalignment orbit plots, all calculated and displayed in real-time. The contact elimination strategy has experimentally been investigated for various values of stator misalignment and initial rotor misalignment. Contrary to intuition but compliant with the parametric study, the experimental results have shown that for the seal under consideration contact can be eliminated through clearance reduction. In Figures 9a-9c the time signals and PSD are shown for decreasing values of clearance. It is clear that the synchronous 1X PSD component is increasing, while the HHO (2X, 3X, etc.) are decreasing with the clearance. Such a behavior is desirable because a stronger synchronous 1X component and weaker HHO indicate superior tracking in the noncontacting mode of seal operation.

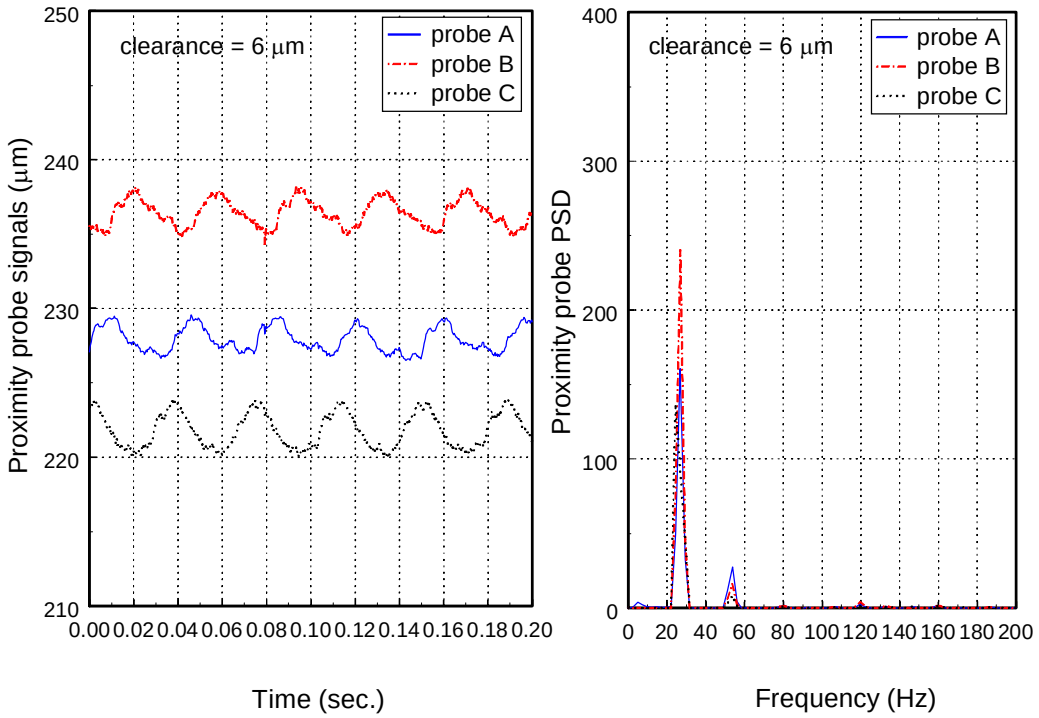

Figure 9a Proximity probe signals and their PSDs for clearance = 6 μm

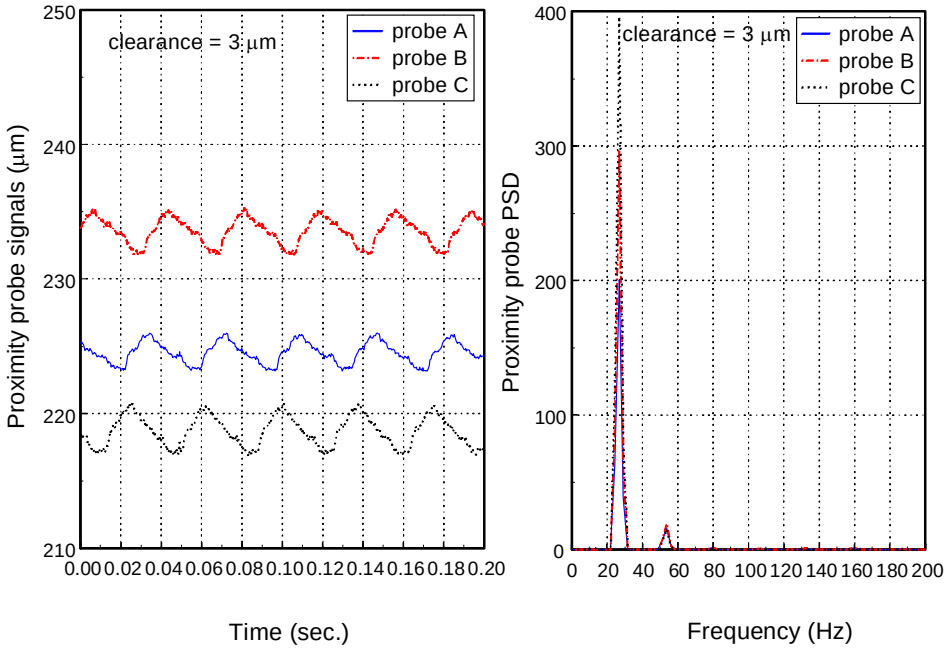

Figure 9b Proximity probe signals and their PSDs for clearance = 3 μm

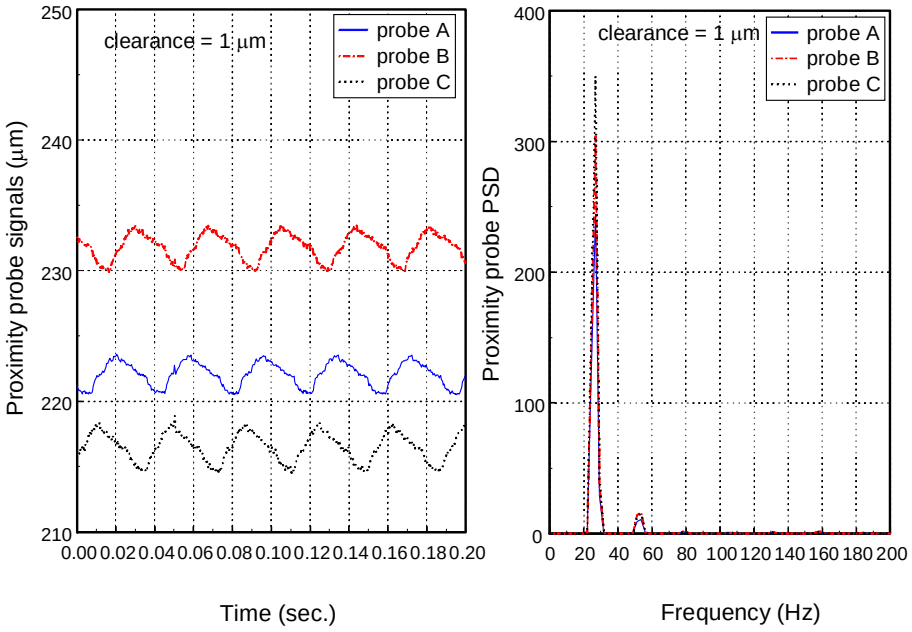

Figure 9c Proximity probe signals and their PSDs for clearance = 1 μm

The orbit plot (Figure 10) is also becoming more organized and closer to circular with a decrease in clearance. This is consistent with a dynamic analysis discussed above.

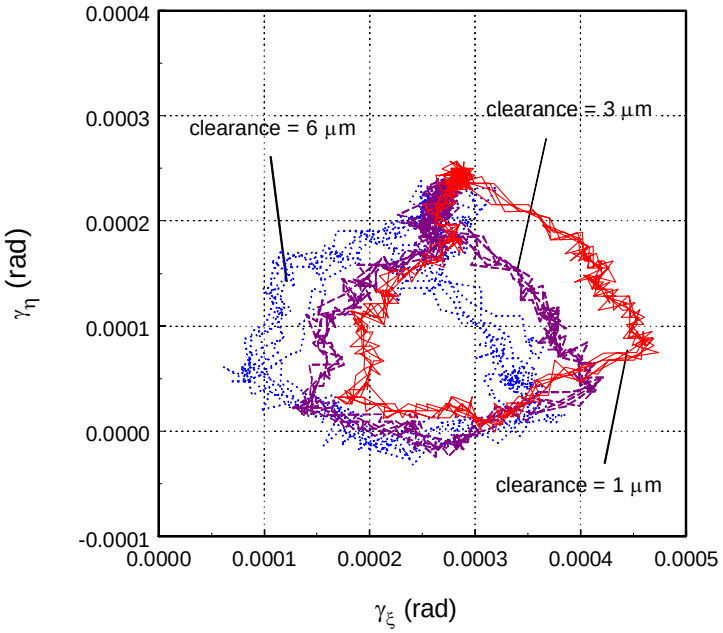

Figure 10 Rotor angular misalignment orbit for different clearances

4. Contact Elimination

The large relative misalignment between seal faces causes the intermittent seal face contact. Controlling seal clearance is the most versatile way of eliminating damaging face contact. A cascade controller that includes two PI feedback control loops has been used. The inner loop is a clearance control loop that maintains a desired clearance set point. Eddy current proximity probes are used to directly measure the seal clearance. Clearance control is accomplished through adjusting the air pressure in the rotor chamber of the seal. The outer loop adjusts desired clearance when contact is detected, i.e., when the variances of the probe signals are different. Experiments have been conducted to test the cascade controller. Results below show that, when coning angle is small (and contrary to intuition) reducing seal clearance can eliminate contact.

Contact elimination results

Experiments are conducted under different stator coning angles, shaft speeds and sealed water pressures, testing if the entire cascade controller is able to eliminate face contact. The results of one of the experiments, where coning angle is 1 mrad, water pressure is 344.8 kPa, shaft speed is 28 Hz, and stator misalignment 2 mrad are plotted in the following set of figures (11-15).

Figure 11 depicts the changes in probe displacement signals obtained when the control is switched on and off. Clearly, the shape and peak-to-peak values of the signals are different for the three probes when control is off but they are almost identical when the control is on.

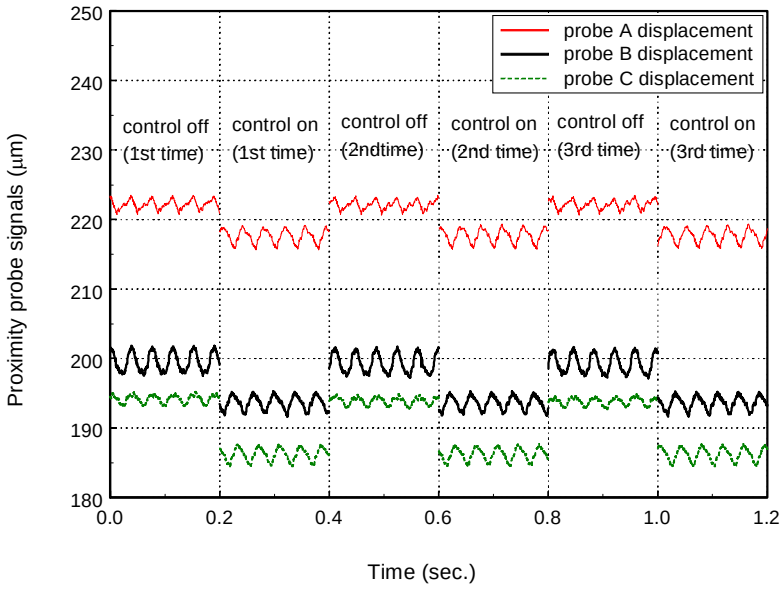

Fig. 11 Proximity probe signals when the control is on and off

It is easier to see these differences from the PSDs of the three probes as plotted in Fig.12, for the respective control on and control off cases. The relative misalignment between the rotor and the stator is smaller when the control is on (Fig. 13).

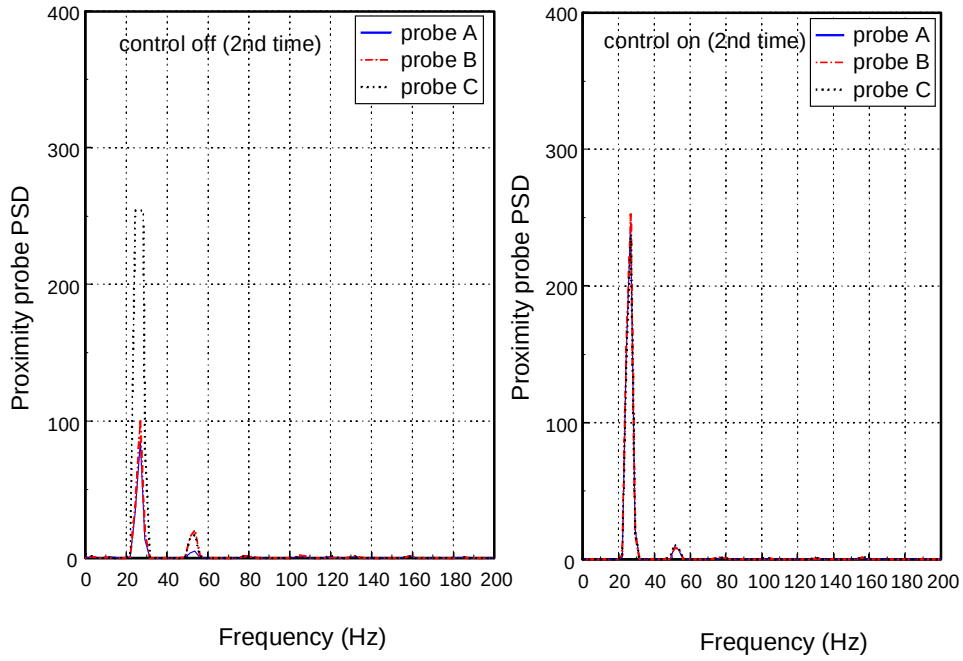

Fig. 12 Proximity probe PSDs when the control is on and off

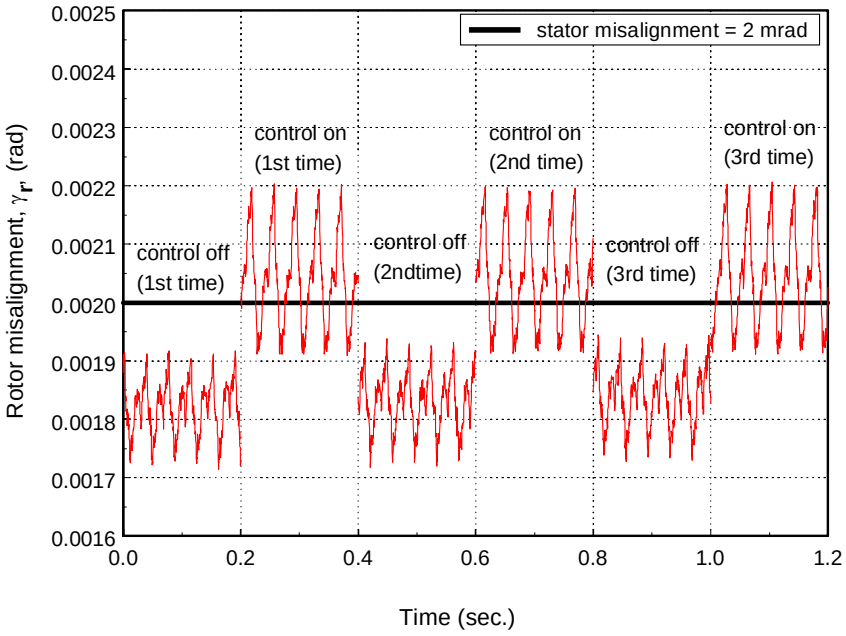

Fig. 13: Rotor misalignment when the control is on and off

The rotor misalignment orbit, indicating the magnitude of the rotor misalignment positioned at its instantaneous precession angle, is plotted in Fig. 14. The orbit becomes more circular for the 'control on' case, and its center moves towards the point that is defined by the stator misalignment and stator angle.

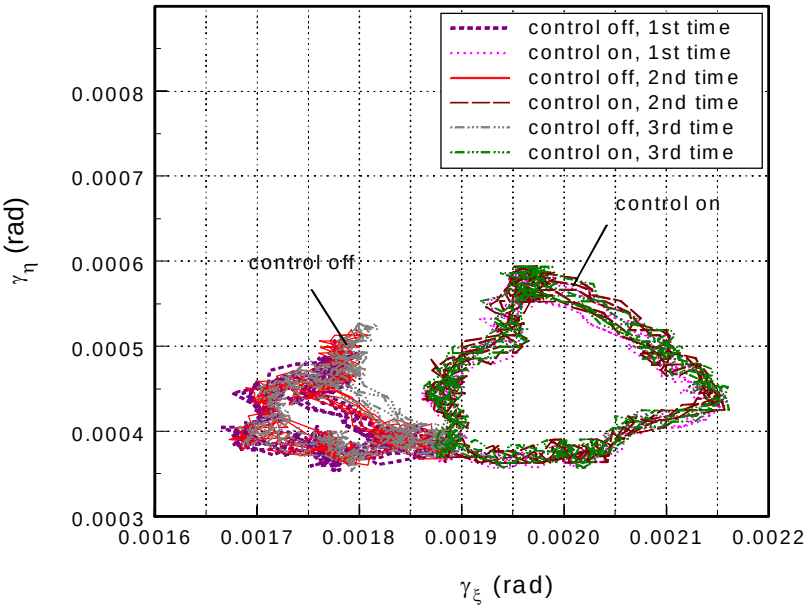

Fig. 14: Rotor angular misalignment orbit for control on and off cases

When the cascade control is 'on' the variance loop drives the system toward better alignment (eliminating the contact), and as can be seen from Fig. 15 it is automatically reduces the clearance. This is an indication that under the tested conditions reducing the clearance does indeed reduce the relative misalignment, as was shown analytically. Figure 15 also shows that clearances calculated from the probe measurements are well correlated and in good agreement with clearances calculated from leakage measurements (assuring that both methods are adequate). The changes in the controller output required (air pressure in the rotor chamber) are very small, demonstrating that the control is well tuned and quite effective.

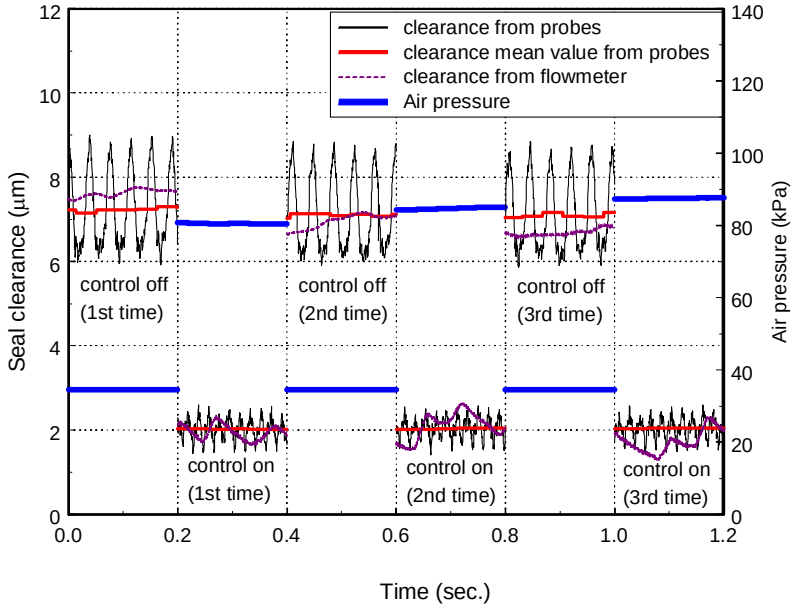

Fig. 15: Seal clearance and air pressure when the control is on and off

The active control is realized by a cascade scheme using two PI control loops. The inner control loop maintains the desired clearance, while the outer loop calculates and dictates the setpoint, based on the contact detecting result. The contact is determined by the appearance of abnormal HHO in the signal of the measured clearance (the output of eddy current proximity probes). These HHO are detected by parameters of the DSP and misalignment orbit for the seal. Once detected, a feedback control loop measuring the probe signal variance differences determines the new target gap, which will eliminate the contact and resume normal noncontacting operations. Also because the leakage is proportional to the clearance cubed, when the control is on the leakage is significantly reduced as well.

In summary, using the proximity probes measurements as feedback in a cascade control loop, interpreting the existence of high harmonics or non-circular orbits as contact, and applying the necessary closing force on the FMR to adjust the clearance, eliminates that contact.

5. Crack Detection

To develop a truly local crack model it is necessary to determine the additional flexibility due the presence of the crack alone. The additional flexibility can then be represented by its own lumped parameter element. A section of a shaft containing a crack of depth, *a*, is shown, under general loading, in Figure 16.

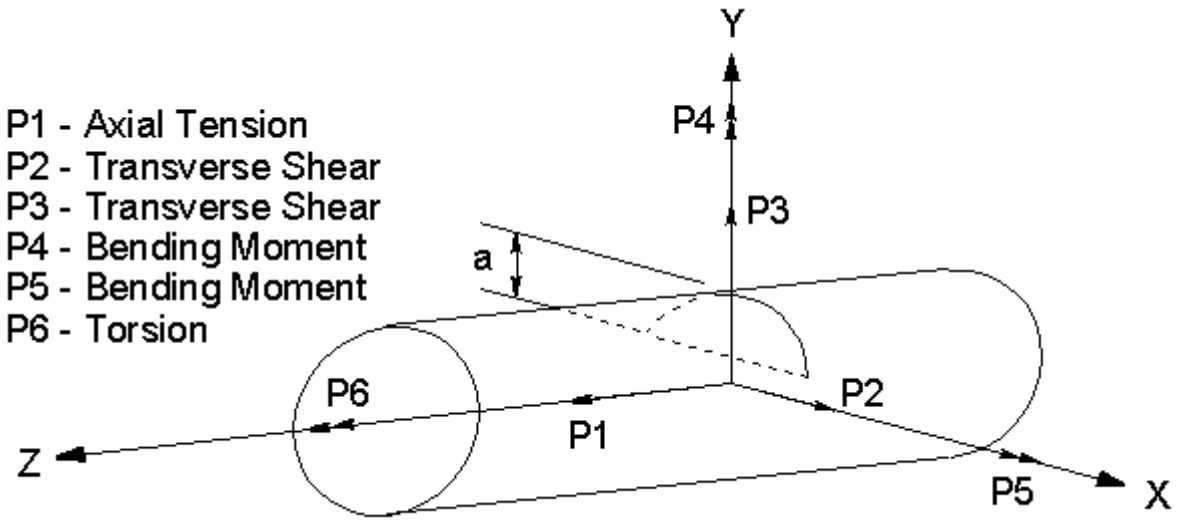

Fig. 16 Shaft section containing a crack

Utilizing the Paris equation and Castigliano's theorem the additional flexibility due to a crack of depth *a*, can be obtained from the strain energy density function. Using a unique complex extended transfer matrix the forced response is computed as a function of shaft speed. The magnitudes plotted in Figure 17 are the radii of the predicted circular 2X tilt responses. It is clear that for an arbitrary shaft speed, the amplitude of the 2X response is predicted to increase as the crack depth increases.

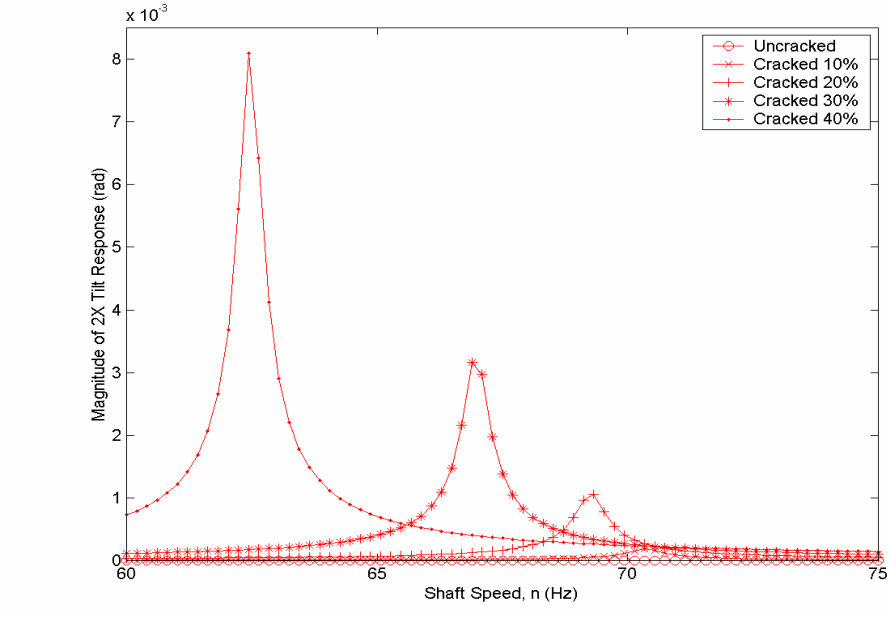

Fig. 17 Local asymmetry model forced 2X response.

To generate experimental plots of the magnitude of the 2X component of the system response as a function of shaft speed, within the selected shaft speed ranges, the following methodology was utilized. The shaft speed was incrementally adjusted via the manual motor control. The DS1102 board took a time sample of the probe data. The power spectral density (PSD) of the time data was computed using Matlab, and the 1X and 2X magnitudes were obtained and stored. This process was repeated over the range of desired shaft speeds for crack depths ranging from 0%-40% of the shaft diameter. A single shaft specimen was utilized in these experiments. The crack depth was incrementally increased for each set of experiments. Figure 18 shows the 2X PSD amplitude of the response provided by one of the probes as a function of shaft speed, for the low and high speed ranges respectively, for crack depths ranging from 0%-40% of the shaft diameter. It is clear from Figure 17 and 18, and Table 1 that the experimental results agree qualitatively quite well with the theoretical model, particularly with the local asymmetry model. Hence, this 2X behavior may provide a strong indication for the presence of a crack.

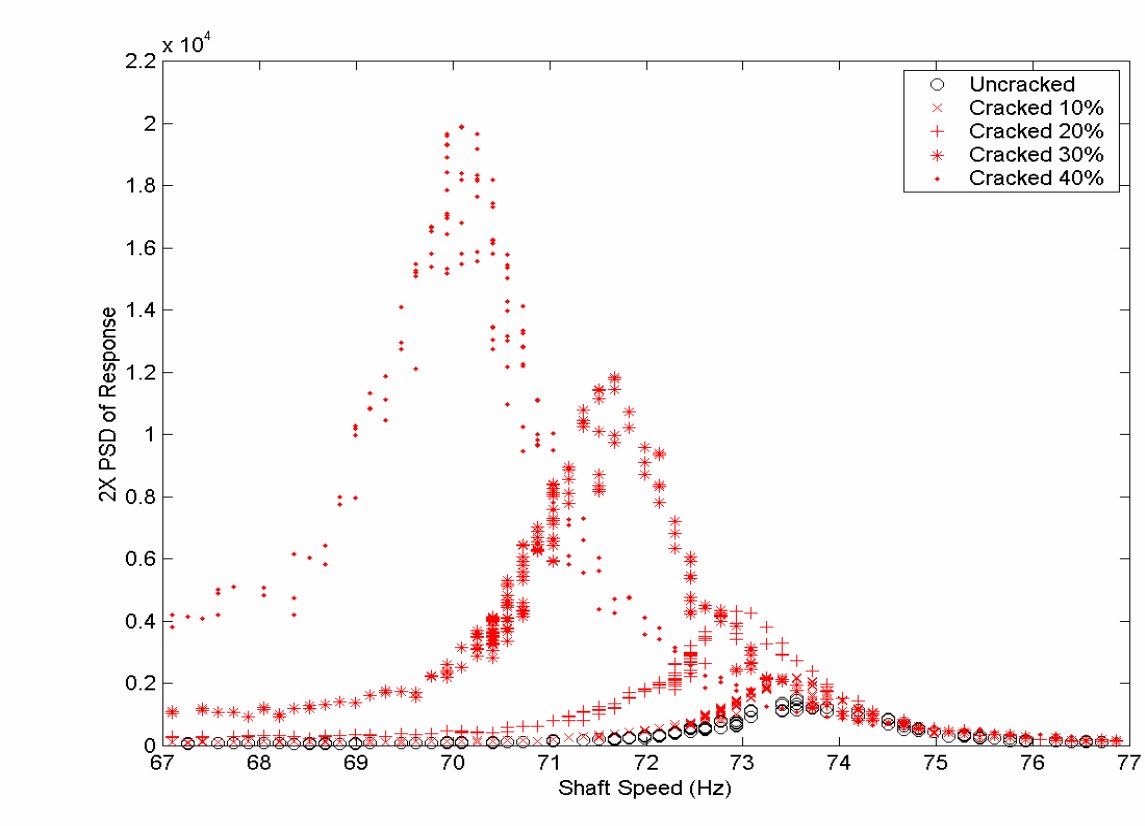

Fig. 18 Experimental 2X response.

Table 1 Comparison of theoretical and Experimental 2X resonance shaft speeds

	Global - Free / Forced	Local - Free / Forced	Experimental
% Cracked	Shaft Speed (Hz)	Shaft Speed (Hz)	Shaft Speed (Hz)
0	70.62 / -	70.62 / -	73.56
10	67.04 / 67.04	70.34 / 70.34	73.50
20	60.55 / 60.55	69.24 / 69.24	72.92
30	52.29 / 52.29	66.97 / 66.97	71.67
40	43.01 / 43.01	62.44 / 62.44	70.09

Tilt Orbit Monitoring

As described above the FMR mechanical face seal monitoring system has the unique capability of obtaining the instantaneous rotor angular response orbit from the signals of the three proximity probes. The predicted behavior of the magnitude of the 2X component of the system response is likewise expected to be experimentally observed. To experimentally observe the effects of the introduction and propagation of the open crack in the crack detection test rig on the 2X component of the time response of the tilt orbit obtained from the monitoring system, the signals are passed through a high pass filter, in the time domain, which removes 1X and lower frequency content. Since, in the absence of contact (the FMR seal is absent), the harmonic components of the signal that are greater than 2X are relatively small, the resulting signal is primarily the 2X harmonic component of the response orbit. Figure 19 shows the 2X content of the tilt orbit, for four depths of the crack near 2X resonance.

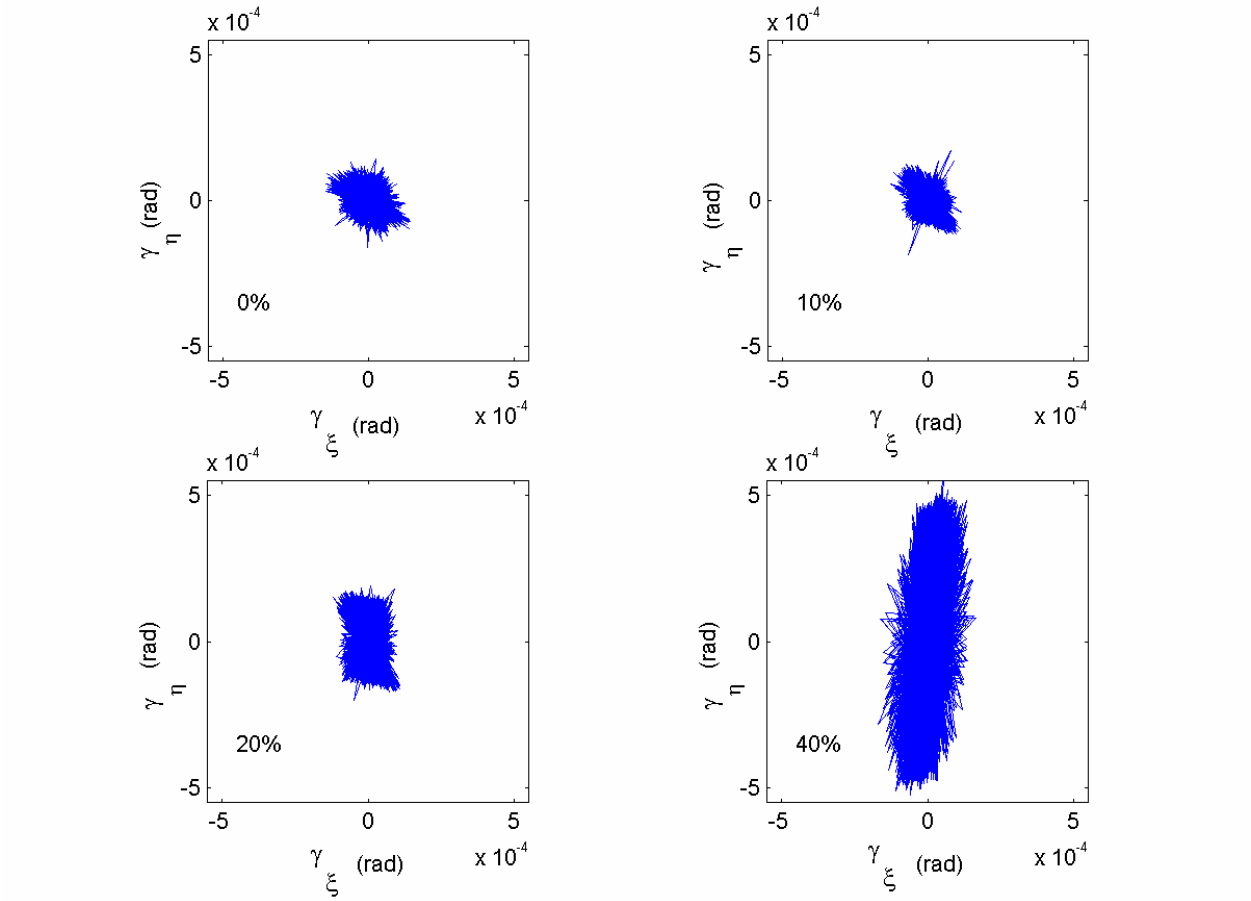

Figure 19 Experimental 2X content of tilt orbit at 71 Hz

In the figure the depth of the crack is indicated, as a percentage of the shaft diameter, in the lower left corner of the axes. It is clear that the increasing crack depth increases the magnitude of the 2X component of the tilt orbit response. The increase in the magnitude of the 2X component of the tilt orbit response is more significant for increasing shaft speeds. The shapes of the 2X component of the tilt orbit responses are not exactly circular.

Since this research is focused on exploring the feasibility of utilizing an existing monitoring system to detect an additional type of system fault, it is important to, at least preliminarily, consider the type of issues that could arise if the monitoring system was used to detect both types of failure simultaneously. The most direct interference that could occur between the two types of fault detection is a scenario in which one type of fault induces a system

response characteristic that influences the response characteristic upon which the monitoring system diagnoses the other type of fault. The seal face contact detection system diagnoses contact based on the relative variance between the three proximity probes signals. Any relative variance in the probe signals will manifest itself in the angular response orbit as a non-circular shape. To observe the characteristics of the orbit shape due to the introduction of the crack into the test rig system, the unfiltered angular response orbits of the system are shown in Figure 20 for shaft speeds which are near the respective 2X resonance shaft speeds, and crack depths ranging from 0%-40%. The orbit shapes at these near 2X resonance speeds demonstrate the most significant influence of the presence of the crack on the system.

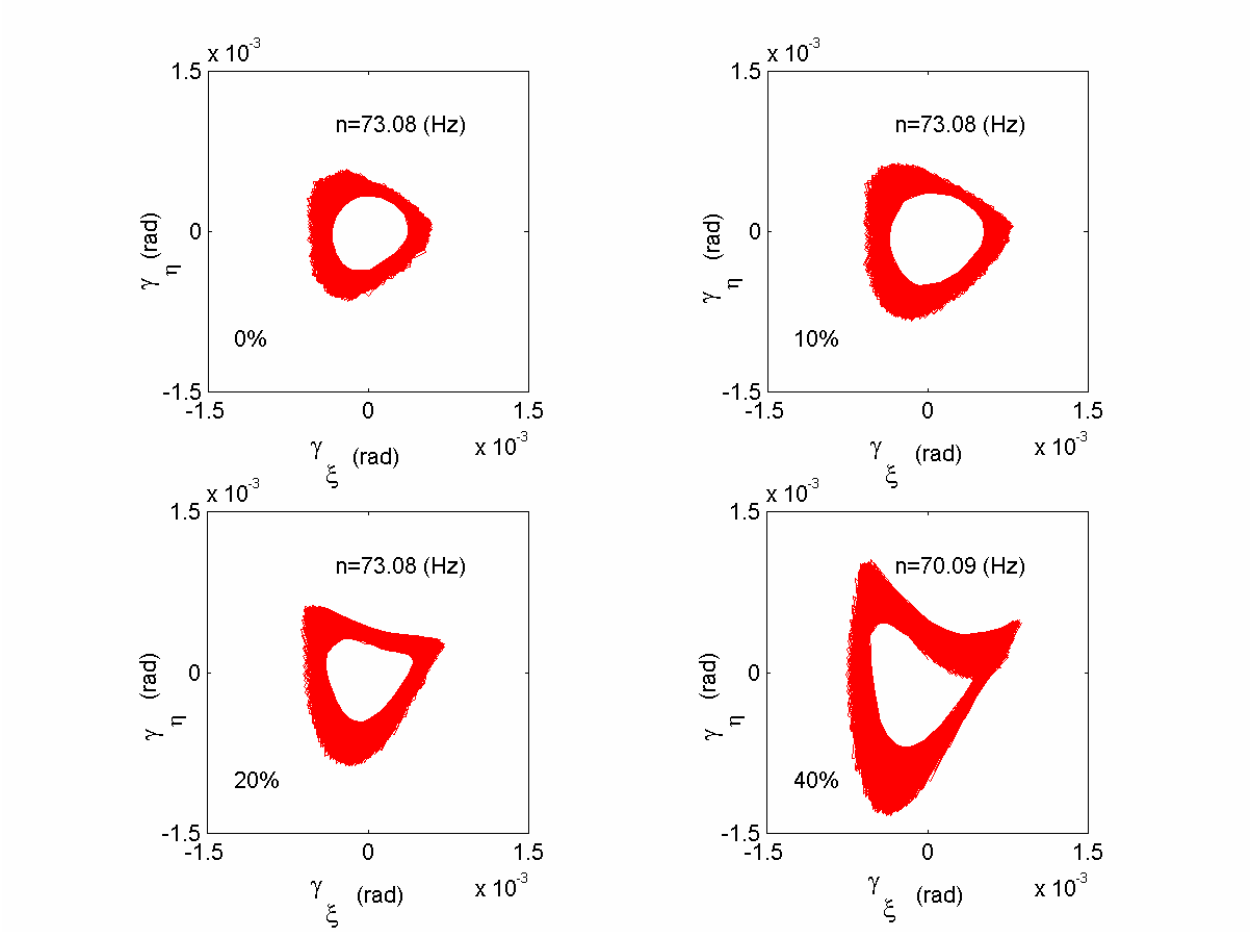

Figure 20. Unfiltered experimental tilt orbit new 2X resonance

These 2X resonance tilt orbits clearly deviate increasingly from a circular shape, which becomes more non-circular for increasing crack depths. The shapes of the tilt orbits for the sealing system when contact is occurring are mostly circular. By observation (e.g., Figure 10), these orbits are distinctly different than the non-circular tilt orbits for the cracked shaft (Figure 20). The non-circular shape of the 2X resonance tilt orbits indicate that relative variance in the probe signals, which is a target observation of the seal face contact detection system, is induced by the presence of a shaft crack. It has also been shown that higher harmonics, one of which (2X) is a target observation for the shaft crack detection system, are induced by seal face contact. This potential interaction, between a shaft crack and seal face contact detection system, raises some questions regarding interference in a simultaneous multi-fault detection system. However, the relative variance in the probe signals induced by the shaft crack is much less significant at shaft speeds that are not near 2X resonance speeds. Also, the higher harmonic responses induced by seal face contact occur for all integer harmonics, not only at the 2X. Furthermore, the clearly non-circular shape of the angular response orbits at 2X resonance speeds may be useful in differentiating between

seal contact and a shaft crack. The specific capabilities of the monitoring system to detect either type of failure, or to discriminate between the two, depend almost entirely on the unique characteristics of the specific system which is under observation.

Future Research

In this research the seal monitoring system was common to both, the contact detection of the seal, and the detection of the presence of a crack in the driving shaft. However, each phenomenon was investigated separately to isolate the behavior, and understand better the physical processes that occur. It is desirable to install the flexibly mounted rotor seal back into the test rig, where now it would ride upon a cracked shaft. The analysis of this coupled problem will have to be developed, and then experimentally investigated. Monitoring of other machine elements, such as failing gears or bearings, could also been added to the investigation.

M-URI PUBLICATIONS (REFERENCES)

Zou, M., and Green, I., "Real-time Condition Monitoring of Mechanical Face Seal" Proceedings of the 24th Leeds-Lyon Symposium on Tribology, London, Imperial College, (Sept. 4-6, 1997) 423-430.

Zou, M., and Green, I., "Clearance Control of a Mechanical Face Seal," **STLE Tribology Transactions, STLE Tribology Transactions, Vol. 42**, No. 3 (July 1999) 535-540, (presented at the ASME-STLE Tribology Conference, Toronto, 1998). Received the *STLE* Walter D. Hodson Award, 2001.

Zou, M., Dayan, J., and Green., I., "Parametric Analysis for Contact Control of a Noncontacting Mechanical Face Seal," **Proceedings of Vibration, Noise & Structural Dynamics, 1999,** Venice, Italy, (28-30 April, 1999) 493-499.

Zou, M., Dayan, J., and Green, I., "Dynamic Simulation and Monitoring of a Noncontacting Flexibly Mounted Rotor Mechanical Face Seal," **IMechE, Proc. Instn. Mech. Engrs, Vol. 214,** No. C9, Part C, (2000) 1195-1206.

Dayan, J., Zou, M., and Green, I., "Sensitivity Analysis for the Design and Operation of a Noncontacting Mechanical Face Seal," **IMechE, Proc. Instn. Mech. Engrs, Vol. 214,** No. C9, Part C, (2000) 1207-1218.

Zou, M., Dayan, J., and Green, I., "Feasibility of Contact Elimination of a Mechanical Face Seal through Clearance Adjustment," **Trans. ASME, Journal of Engineering for Gas Turbines and Power, Vol. 122,** No. 3, (July 2000) 478-484.

Dayan, J., Zou, M., and Green, I., "Contact Elimination in Mechanical Face Seals Using Active Control" **IEEE Transactions on Control Systems Technology**, **Vol. 10**, No. 3, (May 2002) 344-354.

Green, I., and Casey, C., "Crack Detection in a Rotor Dynamic System by Vibration Monitoring - Part I: Analysis," Preprint GT2003-38659, ASME Turbo Expo 2003, Power for Land, Sea, and Air, June 16-19, 2003, Atlanta, Georgia, USA. In press, **ASME Trans., Journal of Gas Turbines and Power.**

M-URI THESES

Min Zou, "Higher Harmonic Oscillations of Triboelements," Ph.D. Thesis, Georgia Tech, March 1999 (currently she is an Associate Professor at the University of Arkansas).

Cody Casey, "Crack Detection in Rotor Dynamic System by Vibration Monitoring," M.S. Thesis, Georgia Tech, June 2000 (with Schlumberger).